Dalton
Transactions

PAPER

View Article Online
View Journal | View Issue

Check for updates

Cite this: *Dalton Trans.*, 2026, **55**, 5217

Received 19th January 2026,
Accepted 5th March 2026

DOI: 10.1039/d6dt00131a

rsc.li/dalton

Synthesis of Mn-bearing layered perovskite-type niobate and its delaminated nanosheet

Yasuo Ebina, * Yuichi Michiue, Nobuyuki Sakai and Takayoshi Sasaki

Layered perovskite-type compounds with the general formula $MCa_2MnNb_3TiO_{13}$ (M = K, Rb), in which Mn^{2+} is incorporated into the A-site of the perovskite layers, were synthesized *via* a unique conventional solid-state reaction. The synthesis was conducted by thoroughly mixing a layered perovskite precursor, $MCa_2Nb_3O_{10}$, with ilmenite-type $MnTiO_3$ in a stoichiometric molar ratio, followed by high-temperature calcination at 1373 K. Compositional and structural characterizations involving elemental analysis and Rietveld refinement confirmed that the perovskite slabs in the host layers are four $[Nb,Ti]O_6$ octahedra thick, with Ca^{2+} and Mn^{2+} ions occupying the A-sites. Ion exchange treatment with an acid solution effectively replaced the interlayer alkali metal ions (K^+ or Rb^+) with protons. Subsequent exfoliation by shaking in an aqueous tetrabutylammonium hydroxide solution yielded a light brown suspension. The colloidal material dispersed was deposited onto a Si substrate surface. Atomic force microscopy (AFM) revealed the presence of numerous micrometer-sized 2D nanosheets with a uniform thickness of approximately 2.0 nm, indicating complete exfoliation into single perovskite layers. Further in-depth analysis *via* in-plane and out-of-plane X-ray diffraction (XRD), as well as X-ray photoelectron spectroscopy (XPS), confirmed that the obtained 2D materials correspond to individual perovskite layers derived from the Mn-substituted parent phase.

1 Introduction

A class of compounds known as layered perovskite oxides has garnered significant attention owing to a wide range of functional properties such as dielectricity, ferroelectricity, and photocatalytic activity based on their diverse compositions and structures.[1–5] Among them, compounds with the general formula $MA_{n-1}B_nO_{3n+1}$ (where M denotes alkali metals such as K, Rb, or Cs; A represents alkaline earth metals such as Ca or Sr; and B corresponds to transition metals such as Ti, Nb, or Ta) are classified as Dion–Jacobson-type layered perovskites.[6–9] A representative member of this series is $KCa_2Nb_3O_{10}$, which features a layered structure consisting of perovskite-type slabs composed of three corner-sharing NbO_6 octahedra stacked along the crystallographic *c*-axis. The interlayer region is occupied by alkali metal cations, which compensate for the negative charge of the perovskite layers. These interlayer cations are readily exchangeable under ambient conditions, enabling the intercalation of various organic molecules or metal complexes to form hybrid nanocomposites.[10–15] Furthermore, this ion-exchangeability allows for the exfoliation of the layered structure into unilamellar 2D nanosheets, which has been an active area of research in recent decades.[16–19] A series of related compounds with homologous structures, in which the thickness of the perovskite slabs varies with the number of NbO_6 octahedra, has also been reported.[7,16,20,21] These compounds are generally represented by the formula $KCa_2Na_{n-3}Nb_nO_{3n+1}$, where n indicates the number of octahedral layers in the perovskite slab. Phases with $n = 3$ or 4 can be synthesized *via* conventional solid-state reactions involving stoichiometric mixing of precursor oxides followed by high-temperature calcination (typically in the range of 1273–1473 K). However, such conventional methods are generally ineffective for synthesizing higher-order phases with $n \geq 5$. Alternatively, these homologous phases can be obtained through a stepwise reaction approach. For example, heating a 1 : 1 molar mixture of $KCa_2Nb_3O_{10}$ and $NaNbO_3$ results in the formation of an $n = 4$ phase, in which one additional NbO_6 octahedral layer is incorporated into the original perovskite framework, as described in the eqn (1).

$$KCa_2Nb_3O_{10} + NaNbO_3 \rightarrow KCa_2NaNb_4O_{13} \qquad (1)$$

Similarly, by adjusting the molar ratio of $NaNbO_3$ to 2, 3, or 4 during thermal treatment, a series of homologous layered oxides with $n = 3–7$ was successfully synthesized. Owing to the fact that the thickness of the perovskite layers in these compounds can be precisely tuned in increments of approximately 0.4 nm—corresponding to the height of a single NbO_6 octahedron—this system has been extensively studied as a model

Research Center for Materials Nanoarchitectonics (MANA), National Institute for Materials Science (NIMS), 1-1 Namiki, Tsukuba, Ibaraki 305-0044, Japan. E-mail: ebina.yasuo@nims.go.jp

platform for investigating structure-property relationships in layered perovskite oxides. We exfoliated the compounds with $n = 3$ to 6 into single-layer nanosheets and investigated their dielectric properties. As a result, we observed a stepwise increase in the relative dielectric constant from ~200 to ~450 with increasing, indicating that these nanosheets exhibit excellent dielectric performance despite their nanometer-scale thickness.[20,22] Furthermore, as indicated in the eqn (2a) and (2b), analogous layered structures can be obtained by employing other perovskite-type oxides, such as $CaTiO_3$ or $SrTiO_3$, demonstrating the versatility of this synthetic approach.[8]

$$KCa_2Nb_3O_{10} + CaTiO_3 \rightarrow KCa_3Nb_3TiO_{13} \tag{2a}$$

$$KSr_2Nb_3O_{10} + SrTiO_3 \rightarrow KSr_3Nb_3TiO_{13} \tag{2b}$$

In a manner analogous to the previously reported approach, homologous phases with the general formula $KCa_{n-1}Nb_3Ti_{n-3}O_{3n+1}$ (n = 4, 5) can be synthesized by tuning the molar ratio of $CaTiO_3$ in the reaction mixture. In these cases, Ca or Sr ions are incorporated into the A-site of the perovskite layers in place of Na ions as in the eqn (1), while Ti is co-substituted with Nb at the B-site. These results indicate that, although the thermodynamic stability of such homologous layered perovskites generally decreases with increasing slab thickness – making their synthesis *via* conventional solid-state methods more difficult – the reactions represented by eqn (1) and (2) enable the formation of higher-order members in the homologous series. This is likely facilitated by the layered perovskite matrix serving as a structural template, allowing for the controlled insertion of additional NbO_6 or TiO_6 octahedra and thereby incrementally increasing the perovskite slab thickness on a layer-by-layer basis. This templating effect may provide a route to access novel layered perovskite compounds with unique compositions and architectures that are otherwise unattainable by conventional synthetic methods. In the present study, we explored whether the synthetic strategy described by eqn (1) and (2) could be extended to ilmenite-type $MnTiO_3$. While layered perovskite oxides exhibit considerable diversity in composition and structure, their A-sites are predominantly occupied by alkali or alkaline earth metal ions. The successful integration of such transition metals into the layered perovskite framework would significantly broaden the functional landscape of these materials, particularly with respect to their magnetic and redox-related properties.

2 Experimental

2.1 Reagents and materials

Chemicals—K_2CO_3, Rb_2CO_3, $CaCO_3$, Nb_2O_5, TiO_2, and MnO (all ≥99.9% purity, supplied by Rare Metallic Co.)—were used for the synthesis. All other chemicals used in this study were of analytical grade or higher. Ultrapure water (Milli-Q, resistivity >18 MΩ cm) was used throughout all experimental procedures. The layered perovskite compounds $KCa_2Nb_3O_{10}$ and $RbCa_2Nb_3O_{10}$, serving as the basic frameworks, were synthesized by mixing K_2CO_3 or Rb_2CO_3, $CaCO_3$, and Nb_2O_5 in a molar ratio of 1.1 : 4 : 3, followed by calcination at 1473 K for 10 h in a platinum crucible.[6,21] The ilmenite-type oxide $MnTiO_3$ was prepared by calcining a stoichiometric mixture of MnO and TiO_2 at 1473 K for 12 h.[23] The target compounds, $KCa_2MnNb_3TiO_{13}$ and $RbCa_2MnNb_3TiO_{13}$, were synthesized by solid-state reaction between $KCa_2Nb_3O_{10}$ or $RbCa_2Nb_3O_{10}$ and $MnTiO_3$ in a 1 : 1 molar ratio, followed by two successive calcination steps at 1373 K for 96 h each. To exchange the interlayer K^+ or Rb^+ ions with protons, 5 g of the resulting product was stirred in 200 cm^3 of 5 M HNO_3 aqueous solution for 72 h.

2.2 Exfoliation

To achieve exfoliation into individual nanosheets, 0.4 g of the acid-treated layered compound $HCa_2MnNb_3TiO_{13}\cdot1.5H_2O$ was dispersed in 100 cm^3 of an aqueous tetrabutylammonium hydroxide (TBAOH) solution and agitated using a mechanical shaker at 170 rpm for 7 days. The concentration of TBAOH was adjusted to be stoichiometrically equivalent to the amount of exchangeable protons in $HCa_2MnNb_3TiO_{13}\cdot1.5H_2O$.

2.3 Film fabrication

To characterize the obtained nanosheets by atomic force microscopy (AFM) and in-plane/out of plane X-ray diffraction (XRD), the nanosheets were deposited onto Si substrates using the Langmuir–Blodgett (LB) technique. Prior to deposition, the Si substrates were cleaned by immersion in a HCl/CH_3OH (1 : 1 v/v) solution for 30 min, rinsed thoroughly with Milli-Q water, immersed in concentrated H_2SO_4 for another 30 min, and finally washed again with Milli-Q water. A 10 cm^3 aliquot of the nanosheet suspension was centrifuged at 1500 rpm for 10 min to remove unexfoliated aggregates. The supernatant (5 cm^3) was then diluted with water to a final volume of 250 cm^3. This diluted suspension was spread onto the water surface in a LB trough, and a monolayer film of nanosheets was transferred onto the substrate at a surface pressure of 10 mN m^{-1} with a lifting speed of 0.0167 mm s^{-1}.

2.4 Characterizations

Powder XRD measurements were carried out using a Rigaku Ultima IV diffractometer equipped with graphite monochromatized Cu Kα radiation source (λ = 0.15405 nm), and a scintillation counter. Crystal structure was analyzed by Rietveld refinement with the program JANA2006.[24] AFM observations were performed using an AFM5000II (Hitachi High-Tech Corp.). In-plane XRD and X-ray absorption near edge structure (XANES) measurements were conducted at beamline BL-6C of the High Energy Accelerator Research Organization (KEK) synchrotron radiation facility. XANES spectra were acquired in transmission mode using pelletized samples prepared by mixing each powder sample with hexagonal boron nitride (h-BN). X-ray photoelectron spectroscopy (XPS) measurements were performed using a PHI Quantes system (ULVAC-PHI). The samples for XPS measurements were prepared by drop-casting a diluted nanosheet suspension onto Si substrates, allowing them to stand for 10 min, removing the excess liquid, and drying the substrates prior to measurement. For chemical analysis, a weighed amount of sample was dissolved in a mixed acid solution of concentrated H_2SO_4 and HF, and the resulting solution was examined using inductively coupled plasma (ICP) atomic emission spectrophotometry (1700HVR, Seiko Instruments Inc.) and atomic absorption spectrophotometry (SpectrAA-20, Varian, Inc.). Water content was deduced from weight loss up to 1273 K using thermogravimetric-differential thermal analysis (TG-DTA, Rigaku TGA-8120).

3 Results and discussion

To evaluate the feasibility of the synthesis route described in eqn (3a) and (3b), equimolar amounts of $MnTiO_3$ were mixed with polycrystalline $KCa_2Nb_3O_{10}$ and $RbCa_2Nb_3O_{10}$. The resulting mixtures were subjected to two successive heat treatments at 1473 K for 96 h each.

$$KCa_2Nb_3O_{10} + MnTiO_3 \rightarrow KCa_2MnNb_3TiO_{13} \tag{3a}$$

$$RbCa_2Nb_3O_{10} + MnTiO_3 \rightarrow RbCa_2MnNb_3TiO_{13} \tag{3b}$$

Fig. 1 displays XRD patterns of the obtained samples. The basal reflection peaks indicate an interlayer spacing of approximately 1.87 nm for both samples, representing an expansion of about 0.4 nm relative to the parent compounds $KCa_2Nb_3O_{10}$ and $RbCa_2Nb_3O_{10}$ (1.48 nm; see Fig. S1). The observed expansion was similar to that occurred in the reactions of (1) and (2), suggesting the formation of the target phase, in which the host perovskite layers are expanded by an additional TiO_6 octahedral unit. Most diffraction peaks observed for the K-containing sample could be indexed to a C-centered orthorhombic unit cell, while those for the Rb-containing sample corresponded to a body-centered lattice. The refined lattice parameters are summarized in Table 1. However, certain reflections were attributed to supercell structures—2 × 2 × 2 for the former and 2 × 2 × 1 for the latter. Such superstructures have been reported in various layered perovskite-type oxides.[6,25] Taking these superstructures into account, all diffraction peaks were successfully assigned to an $n = 4$ member of a homologous series, indicating that the target phase was obtained as a single-phase product. As a control experiment, direct synthesis of the target phase was attempted using stoichiometric mixtures of carbonates and oxides (Rb_2CO_3, $CaCO_3$, MnO, TiO_2, Nb_2O_5). The results revealed the formation of a multiphase product containing Mn_3O_4, $CaMnO_3$, and other impurities (Fig. S2). These results suggest that the synthetic route described in eqn (3), involving precursor phases of lower n values, is more effective for preparing the higher-order target phase.

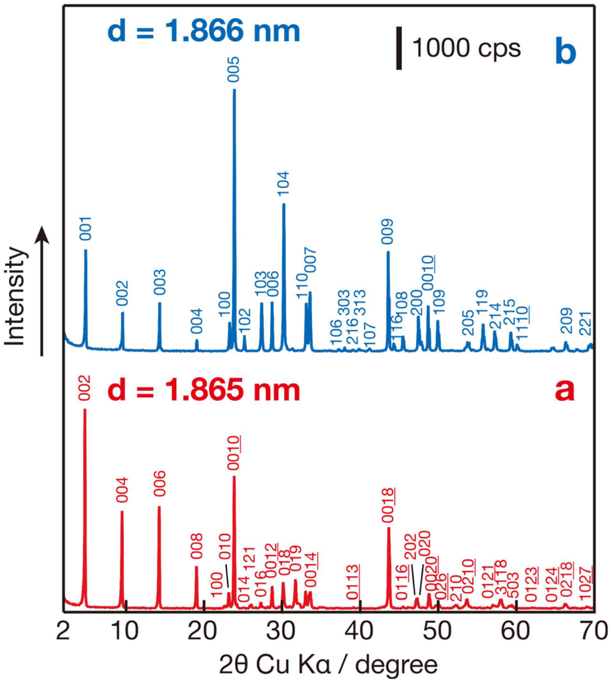

Fig. 1 Powder XRD patterns of (a) $KCa_2MnNb_3TiO_{13}$ and (b) $RbCa_2MnNb_3TiO_{13}$.

Next, the obtained materials were treated with acid solutions to replace the interlayer K^+ or Rb^+ ions with protons. Fig. 2 presents XRD patterns of the acid-treated samples. The lattice parameters of the sample derived from the K-form were determined to be $a = 0.38374(5)$ nm and $c = 2.0092(3)$ nm, indicating an expansion of the interlayer spacing by approximately 0.13 nm. A similar XRD profile was also observed for the acid treatment sample prepared from the Rb form (Fig. S3). This variation in lattice constants is consistent with those reported for Dion–Jacobson-type layered perovskites such as $KCa_2Nb_3O_{10}$, and is attributed to the intercalation of oxonium ions into the interlayer region.[7] Moreover, TG-DTA revealed the presence of approximately 1.5 mol of interlayer water per formula unit (Fig. S4), which is also in good agreement with previously reported acid-exchanged products of $KCa_2Nb_3O_{10}$.[26] Table 2 summarizes the results of elemental analysis before and after the proton exchange process.

For the as-synthesized samples, the elemental molar ratios, normalized to Nb = 3, were approximately (K or Rb) : Ca : Mn : Nb : Ti = 1 : 2 : 1 : 3 : 1 for both the K- and Rb-containing compositions, which is consistent with the nominal target stoichiometry. In contrast, after acid treatment, the

Table 1 Lattice parameters of layered perovskite

Nominal composition	a/nm	b/nm	c/nm
$KCa_2MnNb_3TiO_{13}$			
(Fundamental)	0.39309(9)[a]	0.38415(8)[a]	3.7311(6)
(Superlattice)	0.7872(1)[a]	0.7684(1)[a]	3.7306(4)
$RbCa_2MnNb_3TiO_{13}$			
(Fundamental)	0.3828(1)[a]	—	1.8658(6)
(Superlattice)	0.7657(3)[a]	—	1.8659(7)
$KCa_2Nb_3O_{10}$	3.8799(8)	0.7719(1)	2.9547(5)

[a] The upper column lists the lattice constants for the fundamental lattice, while the lower column indicates the lattice parameters based on the superlattice structures, if any.

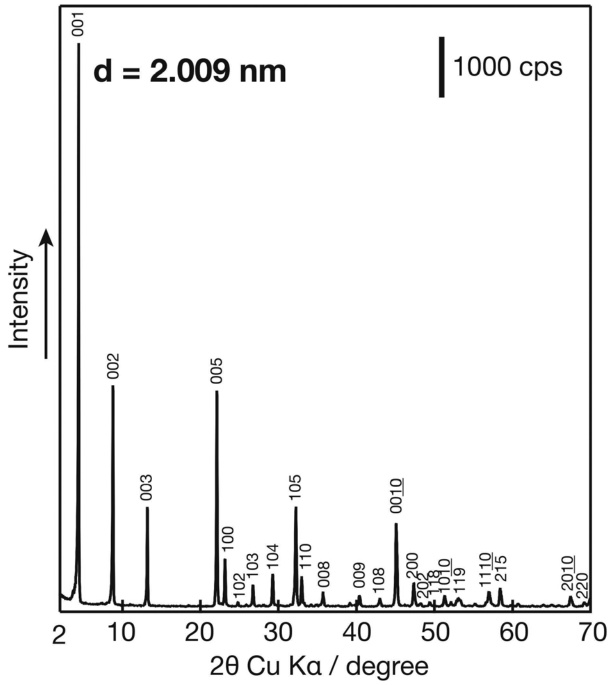

Fig. 2 Powder XRD pattern of the acid-treated product from $KCa_2MnNb_3TiO_{13}$.

elemental ratios of Ca, Mn, Nb, and Ti in the Rb-containing sample remained largely unchanged, whereas Rb became nearly undetectable, indicating that Rb^+ ions were almost completely exchanged with oxonium (H_3O^+) ions. On the other hand, in the K-containing sample, approximately 30% of the initial K^+ ions remained after the proton-exchange treatment, and the contents of Ca and Mn were lower than the ideal stoichiometry. This behavior has also been observed in the synthesis of compounds such as $KCa_2NaNb_4O_{13}$, described by eqn (1), and is understood as a result of partial incorporation of K^+ ions into the A-sites of the perovskite layers during solid-state synthesis. The excess Ca^{2+} and Mn^{2+} ions may then be accommodated in the interlayer region, and involve the proton exchange. In contrast, due to the larger ionic radius of Rb^+, such incorporation into the A-sites was not the case, which leads to a composition closer to the ideal layered perovskite structure in the Rb-containing sample. XANES measurements were performed on both the K-form and H-form samples. Comparison with reference Mn oxides confirmed that Mn remains in the divalent oxidation state throughout the solid-state synthesis and subsequent the proton-exchange processes (Fig. S5). This result is consistent with charge balance based on the nominal composition.

Based on these findings, Rietveld refinement was carried out for more quantitative structural characterization. Since the K-containing sample required a doubled unit cell along the *c*-axis relative to the Rb-containing sample, and considering the structural complexity arising from the solid solution behavior of K^+, Ca^{2+}, and Mn^{2+} occupying both the interlayer and A-sites in the perovskite framework, structure refinement was performed on the Rb-containing sample, which is expected to have a simpler and more ordered structure. Specifically, superstructure features suggested by lattice parameter analysis were disregarded, and instead a model based on a fundamental layered perovskite framework was adopted, referring to previously reported structurally similar compounds.[27] Refined occupancies and atomic displacement parameters may be affected by this simplification of the subcell model, but are reliable enough to discuss the basic feature of the structure. In this model, Ca^{2+} and Mn^{2+} occupy the A-sites within the host perovskite layers at a molar ratio of 2 : 1 as a whole, while Nb^{5+} and Ti^{4+} occupy the B-sites at a molar ratio of 3 : 1. As shown in Fig. 3 and Table 3, satisfactory refinement results were obtained, confirming the successful synthesis of the targeted layered perovskite structure with Mn^{2+} incorporated into the A-sites. In this refinement, fitting was performed with $MnTiO_3$ included as an impurity phase. Its refined with a phase fraction of 3.3%, indicates the almost full reaction of $MnTiO_3$ according to eqn (3b). Although the initial structural model assumed a solid solution of Nb^{5+} and Ti^{4+} with a molar ratio of 3 : 1, the refinement process revealed a pronounced redistribution of Nb^{5+} ions. Specifically, Nb^{5+} progressively accumulated at the B-site positions located closer to the surface of the perovskite layer, ultimately resulting in 100% occupation of these sites by Nb^{5+} (denoted as Nb(2)). In contrast, the B-sites situated nearer to the center of the perovskite layer (Nb(1), Ti(1)) converged to a mixed-occupancy configuration in which Nb^{5+} and Ti^{4+} form a solid solution. This site preference is plausibly attributed to electrostatic considerations based on Pauling's principle.[28] In the present perovskite-related structure, the A-sites within the perovskite layer are occupied by divalent Ca^{2+}/Mn^{2+} cations, while the interlayer region is filled with monovalent Rb^+ cations. Consequently, Nb^{5+} cations are expected to preferentially occupy B-sites adjacent to the interlayer region to stabilize the local charge balance, leading to

Table 2 Elemental analysis results and molar ratios of each layered perovskite

Nominal composition	K or Rb	Mn	Ca	Nb	Ti
$KCa_2MnNb_3TiO_{13}$	6.7 (1.00)	10.5 (1.03)	15.7 (1.95)	57.2 (3.00)	10.8 (0.95)
Acid-exchanged product from K-form	3.3 (0.31)	9.6 (0.89)	16.5 (1.93)	60.7 (3.00)	11.1 (0.91)
$RbCa_2MnNb_3TiO_{13}$	12.3 (0.99)	10.0 (1.06)	15.0 (2.02)	52.8 (3.00)	10.3 (0.97)
Acid-exchanged product from Rb-form	0.6 (0.04)	10.9 (1.02)	16.8 (1.99)	60.1 (3.00)	11.6 (0.96)

The values are given in wt%. The values in parentheses represent the molar ratios normalized with Nb = 3.00.

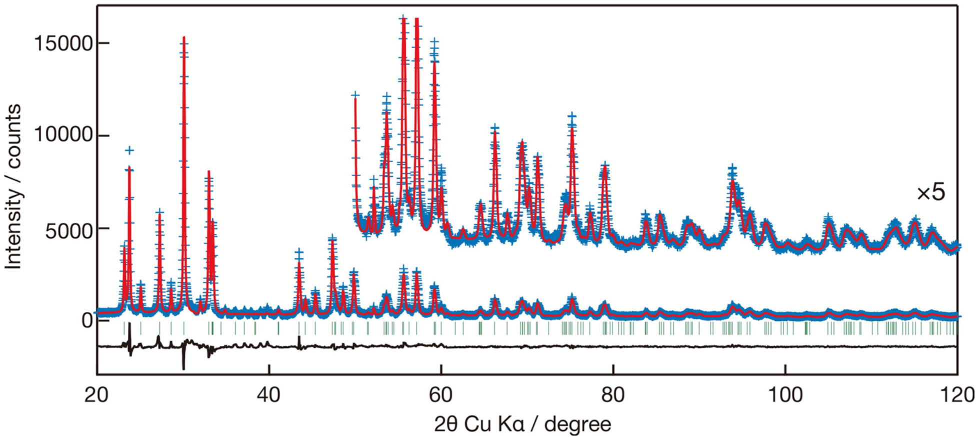

Fig. 3 Structure refinement of X-ray powder diffraction data for $RbCa_2MnNb_3TiO_{13}$. Blue: observed, red: calculated, green: Bragg reflections, black: the difference.

Table 3 Structural parameters from crystal structure refinement for $RbCa_2MnNb_3TiO_{13}$ in space group *P*4/*mmm* (123)

	x	*y*	*z*	Occ.	*U*	Site
Nb(1)	0	0	0.10461(13)	0.5	0.0037(7)	2
Nb(2)	0	0	0.32929(10)	1.0	0.0149(7)	2
Ti(1)	0	0	0.10461(13)	0.5	0.0037(7)	2
Ca(1)	0.5	0.5	0	0.89(6)	0.034(3)	1
Ca(2)	0.5	0.5	0.2207(2)	0.56(3)	0.046(2)	2
Mn(1)	0.5	0.5	0	0.11(6)	0.034(3)	1
Mn(2)	0.5	0.5	0.2207(2)	0.44(3)	0.046(2)	2
Rb(1)	0.5	0.5	0.5	1.0	0.0505(16)	1
O(1)	0	0	0	1.0	0.076(2)	1
O(2)	0	0.5	0.1034(8)	1.0	0.076(2)	4
O(3)	0	0	0.1977(8)	1.0	0.076(2)	2
O(4)	0.5	0	0.3051(6)	1.0	0.076(2)	4
O(5)	0	0	0.4136(10)	1.0	0.076(2)	2

a = 0.3837 nm, c = 1.872 nm, V = 0.27557(1) nm^3, R_p = 8.03%, R_{wp} = 11.04%, R_e = 4.54%, S = 2.43.

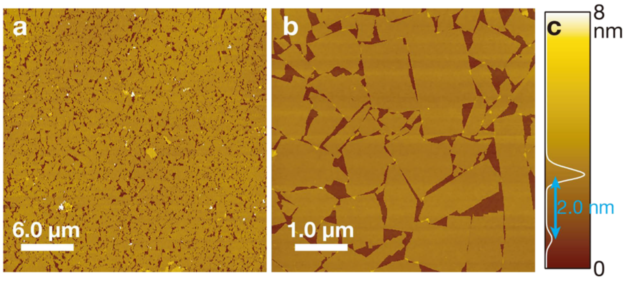

Fig. 4 AFM observation data of $Ca_2MnNb_3TiO_{13}$ nanosheets deposited on a Si substrate. (a) and (b) topographic image and (c) height histogram.

the observed enrichment of Nb^{5+} near the perovskite layer surface.

Subsequently, we examined the exfoliation of the prepared layered perovskite into unilamellar nanosheet. When the acid-treated product derived from the Rb-form, $HCa_2MnNb_3TiO_{13}·1.5H_2O$, was vigorously agitated with an aqueous TBAOH solution, the mixture transformed into a light brown colloidal suspension (Fig. S6). The colloidally dispersed sample was deposited onto a Si substrate *via* the LB technique and subsequently examined by AFM (Fig. 4). The AFM images revealed a large number of rectangular, ultrathin, sheet-like structures. The image provides further evidence for uniform and unilamellar nature of the nanosheet. The height profile histogram (Fig. 4c) exhibited two distinct peaks: one corresponding to the height of the Si substrate and the other to that of the nanosheets, indicating a uniform thickness for the exfoliated perovskite layers. The nanosheet thickness was estimated to be approximately 2.0 nm. This value is in close agreement with the theoretical thickness of 1.859 nm, calculated from the outermost O–O distance in a single perovskite layer as determined by Rietveld refinement, thereby confirming successful exfoliation into individual monolayers. The slightly larger experimental thickness compared to the calculated value is commonly observed in various nanosheet systems and is attributed to the presence of surface-adsorbed water molecules.[29–32]

To examine the crystal structure, in-plane XRD measurements were performed on the monolayer film of $Ca_2MnNb_3TiO_{13}$ nanosheets deposited on the substrate. As shown in Fig. 5, sharp diffraction peaks indicative of high crystallinity were observed, and these peaks could be indexed to a 2D square lattice with a lattice parameter of a = 0.38372(4) nm. This result clearly demonstrates that the fundamental perovskite lattice is preserved after exfoliation into nanosheets.

The out-of-plane XRD pattern was measured in the Bragg–Brentano geometry using a powder X-ray diffractometer (Fig. 6) and exhibited characteristic oscillatory scattering features. The continuous nature of the diffraction profile suggests the absence of repeating periodicity along the thickness (*c*-axis) direction. The observed oscillations are attributed to structural architecture across the nanosheet thickness. To validate this interpretation, the scattering intensity along the *z*-direction of monolayer perovskite nanosheets was calculated based on the

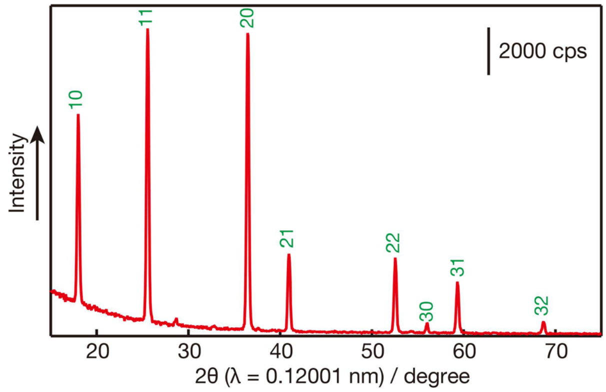

Fig. 5 In-plane XRD pattern of a monolayer film of $Ca_2MnNb_3TiO_{13}$ nanosheets deposited on a Si substrate using the LB method.

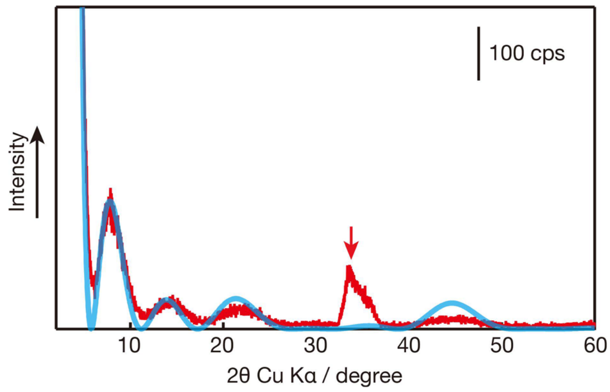

Fig. 6 Out-of-plane XRD pattern of $Ca_2MnNb_3TiO_{13}$ nanosheets monolayer on a Si substrate using the LB method. Red: observed, cyan: calculated. The part indicated by the arrow corresponds to the hump relating to the Si substrate.

atomic coordinates obtained from the aforementioned Rietveld refinement, according to the eqn (4) and (5) below.[21,33] The resulting simulated profile closely reproduced the experimental profile.

$$F_{00l} = \sum_j f_j e^{2\pi i (2z_j \sin\theta f/\lambda)} \tag{4}$$

$$I_{00l} = \frac{1+\cos^2\theta}{\sin^2\theta\cos\theta} F_{00l} F^{*}_{00l} \tag{5}$$

Here, F_{00l} and I_{00l} denote the structure factor and the scattering intensity of a single-layer perovskite nanosheet along the 00l direction, respectively; f_j and z_j denote the atomic scattering factor and the z-coordinate of the j-th atom. θ is the diffraction angle and λ is the X-ray wavelength (Cu Kα, λ = 0.15405 nm). This agreement supports the conclusion that the perovskite layer is composed of four corner-sharing [Nb,Ti]O_6 octahedra, indicating that the perovskite framework is retained along the layer normal.

Fig. 7 shows the wide-scan XPS spectrum of $Ca_2MnNb_3TiO_{13}$ nanosheets obtained from the Rb-containing precursor (Fig. S7). The elemental composition of each nanosheet, determined from the integrated peak areas and normalized to Nb = 3.00, is summarized in Table 4.

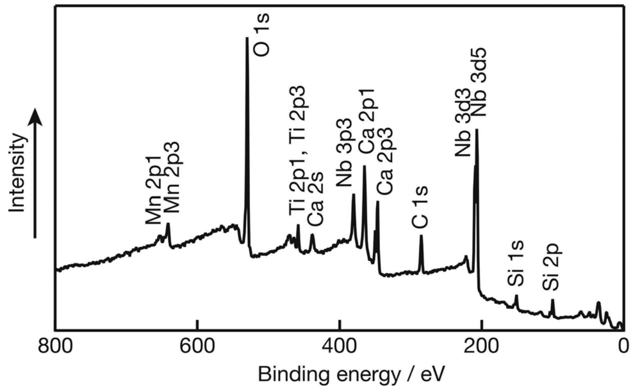

Fig. 7 X-ray photoelectron spectroscopy of $Ca_2MnNb_3TiO_{13}$ nanosheet.

Table 4 Elemental ratios of each $Ca_2MnNb_3TiO_{13}$ nanosheet estimated from XPS

	K	Rb	Ca	Mn	Nb	Ti
From K-form	0.05	—	2.15	0.88	3.00	1.17
From Rb-form	—	0.00	2.03	1.11	3.00	1.10

XPS analysis detected Mn signals in nanosheets derived from both K- and Rb-containing layered perovskites. The nanosheets obtained from the Rb-based precursors exhibited no detectable Rb signal, and the elemental ratios of Ca, Nb, Ti, and Mn were consistent with those determined by elemental analysis after ion exchange. This confirms that the perovskite layer framework was preserved during the exfoliation process. In contrast, nanosheets derived from the K-containing samples exhibited residual K signals and a lower Mn content. These findings are in agreement with the post-ion-exchange elemental analysis, suggesting that a fraction of the K ions is incorporated into the perovskite layers and remains even after acid treatment and delamination.

4 Conclusions

A new class of layered perovskite oxides, $KCa_2MnNb_3TiO_{13}$ and $RbCa_2MnNb_3TiO_{13}$, was successfully synthesized by calcining the precursors $KCa_2Nb_3O_{10}$ or $RbCa_2Nb_3O_{10}$ with illmenite-type $MnTiO_3$. Compositional and structural characterizations confirmed that these compounds belong to the Dion–Jacobson series of layered perovskites. The original three-layer perovskite slabs composed of corner-sharing NbO_6 octahedra were expanded through the incorporation of $MnTiO_3$, forming a novel four-layer perovskite structure comprising mixed [Nb,Ti]O_6 octahedra. To the best of our knowledge, there have been no prior reports of Dion–Jacobson type layered perovskite oxides containing Mn ions at the A-site, and the synthetic route developed in this study offers a promising strategy to expand the compositional diversity of layered perovskites. Furthermore, proton exchange followed by exfoliation enabled the isolation of perovskite nanosheets with a thickness corresponding to four octahedral layers, while retaining the original perovskite framework. The preservation of the perovskite architecture in the exfoliated nanosheets was verified by AFM, in-plane and out-of-plane XRD, and XPS analyses. These findings demonstrate that the present synthetic approach is an effective strategy for the rational design of functional layered perovskite oxides and their corresponding nanosheet derivatives.

Conflicts of interest

There are no conflicts to declare.

Data availability

All data supporting this study are available within the article and its supplementary information (SI). Supplementary information is available. See DOI: https://doi.org/10.1039/d6dt00131a.

Acknowledgements

This work was supported by World Premier International Research Center Initiative (WPI), Ministry of Education, Culture, Sports, Science and Technology (MEXT), Japan, and CREST of the Japan Science and Technology Agency (JST) (grant no. JPMJCR22B1), Japan. The in-plane XRD measurements were performed under the approval of the Photon Factory Program Advisory Committee (Proposal No. 2024G501). This work was supported by "Advanced Research Infrastructure for Materials and Nanotechnology in Japan (ARIM)" of the MEXT. Proposal Number JPMXP1225NM5176. We also acknowledge technical supports by the Surface and Bulk Analysis Unit in NIMS for ICP-OES.

References

1 T. Taniguchi, L. Nurdiwijayanto, R. Ma and T. Sasaki, *Appl. Phys. Rev.*, 2022, **9**, 021313.
2 T. Wang, C. N. Henderson, T. I. Draskovic and T. E. Mallouk, *Chem. Mater.*, 2014, **26**, 898–906.
3 B.-W. Li, M. Osada, Y. Ebina, T. C. Ozawa, R. Ma and T. Sasaki, *Appl. Phys. Lett.*, 2010, **96**, 182903.
4 C. Chen, H. Ning, S. Lepadatu, M. Cain, H. Yan and M. J. Reece, *J. Mater. Chem. C*, 2015, **3**, 19–22.
5 A. Kudo and E. Kaneko, *J. Mater. Sci. Lett.*, 1997, **16**, 224–226.
6 M. Dion, M. Ganne and M. Tournoux, *Mater. Res. Bull.*, 1981, **16**, 1429–1435.
7 A. J. Jacobson, J. W. Johnson and J. T. Lewandowski, *Inorg. Chem.*, 1985, **24**, 3727–3729.
8 R. A. M. Ram and A. Clearfield, *J. Solid State Chem.*, 1991, **94**, 45–51.
9 J. Gopalakrishnan and V. Bhat, *Mater. Res. Bull.*, 1987, **22**, 413–417.
10 R. Uppuluri, A. S. Gupta, A. S. Rosas and T. E. Mallouk, *Chem. Soc. Rev.*, 2018, **47**, 2401–2430.
11 A. J. Jacobson, J. W. Johnson and J. T. Lewandowski, *Mater. Res. Bull.*, 1987, **22**, 45–51.
12 F. Shao, M. Zhuo, G. Han, X. Zhang, L. Liu, T. Tao and Z. Tong, *Micro Nano Lett.*, 2013, **8**, 788–791.
13 Y. Song, N. Iyi, T. Hoshide, T. C. Ozawa, Y. Ebina, R. Ma, N. Miyamoto and T. Sasaki, *Chem. Commun.*, 2015, **51**, 17068–17071.
14 Y. Song, N. Iyi, T. Hoshide, T. C. Ozawa, Y. Ebina, R. Ma, S. Yamamoto, N. Miyamoto and T. Sasaki, *Dalton Trans.*, 2018, **47**, 3022–3028.
15 N. Sakai, R. Uppuluri, N. Iyi, Y. Ebina, R. Ma and T. Sasaki, *Langmuir*, 2025, **41**, 24957–24962.
16 M. M. J. Treacy, S. B. Rice, A. J. Jacobson and J. T. Lewandowski, *Chem. Mater.*, 1990, **2**, 279–286.
17 Y.-S. Han, I. Park and J.-H. Choy, *J. Mater. Chem.*, 2001, **11**, 1277–1282.
18 Y. Ebina, T. Sasaki and M. Watanabe, *Solid State Ionics*, 2002, **151**, 177–182.
19 S. Ohisa, T. Hikichi, Y.-J. Pu, T. Chiba and J. Kido, *ACS Appl. Mater. Interfaces*, 2018, **10**, 27885–27893.
20 B.-W. Li, M. Osada, Y. Ebina, T. C. Ozawa, R. Ma and T. Sasaki, *Appl. Phys. Lett.*, 2010, **96**, 182903.
21 Y. Ebina, K. Akatsuka, K. Fukuda and T. Sasaki, *Chem. Mater.*, 2012, **24**, 4201–4208.
22 M. Osada and T. Sasaki, *Int. J. Appl. Ceram. Technol.*, 2012, **9**, 29–36.
23 A. M. Arévalo-López and J. P. Attfield, *Phys. Rev. B: Condens. Matter Mater. Phys.*, 2013, **88**, 104416.
24 V. Petříček, M. Dušek and L. Palatinus, *Z. Kristallogr.*, 2014, **229**, 345–352.
25 Z.-H. Liang, K.-B. Tang, Q.-W. Chen and H.-G. Zheng, *Acta Crystallogr., Sect. E:Struct. Rep. Online*, 2009, **65**, i44.
26 A. J. Jacobson, J. T. Lewandowski and J. W. Johnson, *Mater. Res. Bull.*, 1990, **25**, 679–686.
27 W. Sugimoto, H. Ohkawa, M. Naito, Y. Sugahara and K. Kuroda, *J. Solid State Chem.*, 1999, **148**, 508–512.
28 L. Pauling, *J. Am. Chem. Soc.*, 1929, **51**, 1010–1026.
29 S. Santos, A. Verdaguer and M. Chiesa, *J. Chem. Phys.*, 2012, **137**, 044201.
30 T. Sasaki, Y. Ebina, Y. Kitami, M. Watanabe and T. Oikawa, *J. Phys. Chem. B*, 2001, **105**, 6116–6121.
31 Y. Omomo, T. Sasaki, L. Wang and M. Watanabe, *J. Am. Chem. Soc.*, 2003, **125**, 3568–3575.
32 K. Fukuda, K. Akatsuka, Y. Ebina, R. Ma, K. Takada, I. Nakai and T. Sasaki, *ACS Nano*, 2008, **2**, 1689–1695.
33 R. C. Reynolds Jr., in *Modern Powder Diffraction*, ed. D. L. Bish and J. E. Post, The Mineralogical Society of America, Washington, DC, 1989, pp. 9–11.